PACS numbers: 61.46.+w, 75.50.Xx
DOI: 10.1070/PU2002v045n11ABEH001209

Submillimeter spectroscopy of electron transitions and the macroscopic quantum tunneling of magnetization in molecular nanoclusters

A A Mukhin, A S Prokhorov, B P Gorshunov,
A K Zvezdin, V D Travkin, M Dressel

Using submillimeter backward-wave-oscillator (BWO) spectroscopy in the 3–33-cm^{-1} frequency range, we have carried out a comprehensive study of the structure of the lower energy levels in the ground multiplet $S = 10$ of the molecular nanocluster Mn_{12}ac, of the interaction of this cluster with the surroundings, and of the relaxation of long-lived spin states. At low temperatures ($T < 2$ K), we have discovered a spectrally inhomogeneous relaxation in the transmission spectra that follows the reversal of the external field. This relaxation manifests itself in a peak and a dip appearing in narrow spectral regions near the inhomogeneously broadened absorption lines corresponding to transitions $|\pm 10\rangle \rightarrow |\pm 9\rangle$. We have shown that this phenomenon is due to the resonant quantum tunneling of magnetization when the energy levels of a cluster with different directions of spin coincide. We have also provided a quantitative description of the novel phenomenon that allows for the time evolution of the population of the spin states and the resonance nature of the relaxation resulting from the thermally activated tunneling of magnetization.

In recent years, molecular chemistry has become very successful in synthesizing large molecules containing magnetic clusters of transition metals [1, 2]. Such clusters are unique objects for studying physical phenomena on the mesoscopic level that is halfway between microscopic and macroscopic phenomena. New materials fabricated from macromolecules exhibit extremely interesting properties, such as bistability on the scale of a single molecule, macroscopic quantum tunneling of magnetization, etc. [2–13]. The study of magnetism in such compounds opens new possibilities for nanomolecular technology, such as developing magnetic memory elements for new information technologies based on supermolecules [14, 15]. The magnetic interaction between clusters is very weak, so that such crystals may be regarded as conglomerates of practically free and identical magnetic subsystems.

An example of a compound of this type that has attracted the greatest interest of researchers is the $Mn_{12}O_{12}(CH_3COO)_{16}(H_2O)_4 \cdot 2CH_3COOH \cdot 4H_2O$ crystals (abbreviated Mn_{12}-acetate, Mn_{12}, or Mn_{12}ac). At low temperatures these nanoclusters behave like monodomain particles with an effective magnetic moment of $20\,\mu_B$ corresponding to the collective spin $S = 10$ of twelve exchange-coupled Mn ions. Due to strong anisotropy, the magnetic moments become frozen and align themselves parallel or antiparallel to the easy axis of the nanocluster, which is parallel to the 4-fold symmetry axis C_4 at temperatures below the energy barrier separating these two states. The magnetic anisotropy is determined by the crystal field, which splits the ground $S = 10$ multiplet and produces an almost quasi-doublet structure in the lower part of the spectrum with states $|\pm m\rangle$ due to the predominance of the axial contribution DS_z^2 with $D < 0$ in the crystal-field Hamiltonian. The height of the energy barrier ($\sim$65 K) between the lower states $|\pm 10\rangle$ determines the thermally activated relaxation of magnetization and the superparamagnetic behavior of nanoclusters with decreasing temperature [9, 12, 16]. At lower temperatures ($T < 3$ K), there is resonant quantum tunneling as the energy levels with $m = -S$ and $m = S - n$ ($n = 0, 1, 2, ...$) move closer to each other (or even coincide) in the magnetic field. This manifests itself in characteristic jumps in the magnetization curves and in anomalies in the magnetization relaxation rate [2, 3, 12]. What makes Mn_{12}ac so special is that in the absence of a transverse field the rate of tunneling between the lower levels is very small because of the very small tunneling splitting. Hence, relaxation is largely determined by the tunneling between the corresponding thermally populated excited levels, which lowers the barrier and 'short-circuits' the corresponding relaxation path. This is what is known as the mechanism of thermally activated tunneling, theoretically described by the Arrhenius law. At even lower temperatures, when the thermal relaxation rate becomes comparable to the tunneling rate, the tunneling becomes thermally assisted, and the Arrhenius law ceases to operate. Finally, complete tunneling between the lowest states sets in [8]. Recent precise magnetic studies of Mn_{12}ac have revealed a fine structure in the tunneling resonances, caused by the fact that not all the energy levels coincide simultaneously; rather, they merge in somewhat different magnetic fields because of the effect of a higher-order crystal field [17–19].

Thus, the special features of the spectrum and the crystal field terms of a nanocluster play an important role in the formation of the nanocluster's magnetic properties and in thermally activated tunneling. In this respect, the use of spectroscopic methods in nanocluster studies is of special interest. Among such methods are electron paramagnetic resonance (EPR) in strong magnetic fields (20–25 T) [20, 21], inelastic neutron scattering [22], and the relatively new method of quasi-optical BWO spectroscopy [23]. This last method enabled us to observe transitions between different levels of Mn_{12}ac in the equilibrium state and to determine the main parameters of the crystal field. We also studied in great detail the intensity and shape of the transition lines and found that for Mn_{12}ac and Fe_8 the shape is Gaussian [24]. It would also be interesting to study relaxation processes by spectroscopic methods. In our report we present the results of studies by submillimeter BWO spectroscopy [25, 26] of Mn_{12}ac nanoclusters that were in either equilibrium or long-lived nonequilibrium states. These studies allowed us for the first time to *spectroscopically* observe relaxation phenomena determined by the resonant tunneling of magnetization [27].

We studied polycrystalline samples of Mn_{12}ac synthesized by a process similar to that described in Ref. [28]. The samples were then pressed into plane-parallel pellets roughly 10 mm in diameter and 1 mm thick. The transmission spectra were measured with a quasi-optical submillimeter BWO spectrometer [25, 26] at frequencies ν ranging from 3 to 33 cm^{-1}, at temperatures ranging from 1.9 to 300 K, and in magnetic fields H up to several teslas. Figure 1 shows some transmission spectra measured in a zero field. As the temperature decreases, a number of absorption lines (*1*, *2*, and *3*) appear in the spectra for $\nu \leqslant 10$ cm^{-1}. The frequencies of these lines remain practically the same as the temperature drops, while the intensities first increase for all modes, and then decrease for modes *2* and *3* and practically vanish, so that at low

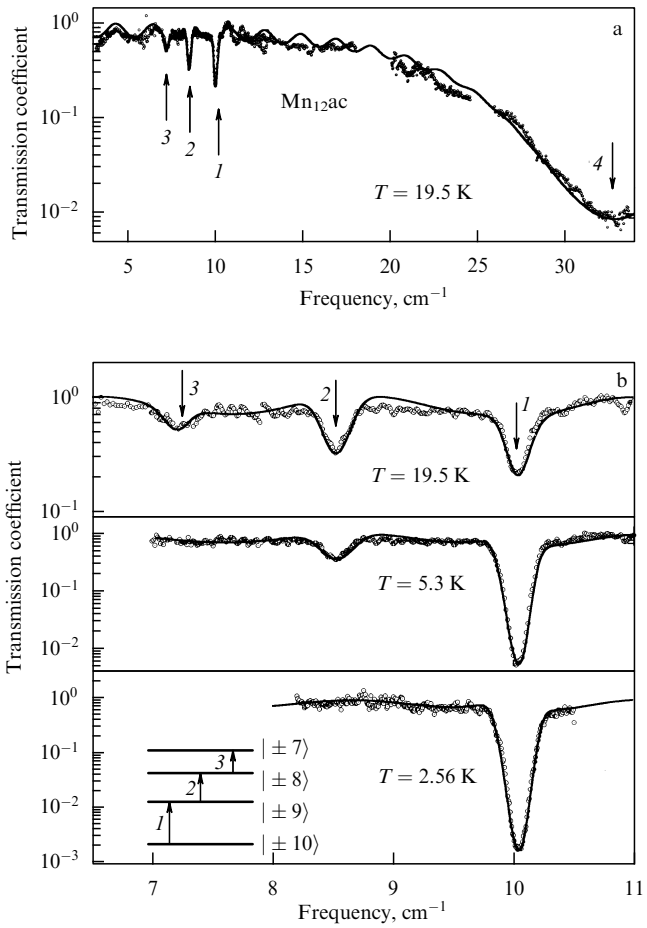

Figure 1. Transmission spectra of a plane-parallel pellet ($d = 1.23$ mm) pressed of a powder of magnetic nanoclusters Mn_{12}ac, at $H = 0$: (a) in a broad frequency range, and (b) near the electronic transitions inside the ground multiplet split by the crystal field. The inset shows the diagram of the low-lying levels with the observed transitions. The points represent experimental data, and the lines, the results of calculations for the Gaussian (modes *1*, *2*, and *3*) and Lorentzian (mode *4*) lineshapes (see the main text).

temperatures the transmission spectra contain only line *1* with the highest frequency $\sim 10\ \mathrm{cm}^{-1}$. We identified the observed lines as transitions between the levels of the ground multiplet $S = 10$ of the nanocluster. The multiplet is split by a crystal field of tetragonal symmetry, whose Hamiltonian is [20–23]

$$H_{\mathrm{cf}} = D_2 S_z^2 + D_4 S_z^4 + B_4^4 \frac{S_+^4 + S_-^4}{2},$$

where the main contribution is provided by the axial part. The high-frequency line *1*, which is present down to the very lowest temperatures, represents the transition between the ground $|\pm 10\rangle$ and excited $|\pm 9\rangle$ doublets; line *2* represents the transition between the excited $|\pm 9\rangle$ and $|\pm 8\rangle$ doublets; etc. (see inset in Fig. 1b). The frequency of the observed transitions makes it possible to immediately determine the parameters of the axial part of the crystal field: $D_2 = -0.389\ \mathrm{cm}^{-1}$ and $D_4 = -7.65 \times 10^{-4}\ \mathrm{cm}^{-1}$ [23].

To determine the characteristics of the transitions (the linewidth and intensities) in greater detail, we simulated the transmission spectra on the basis of Fresnel formulas for transmission through a plane-parallel layer [29, 25, 26] with allowance for the frequency dispersion of the permeability

$$\mu^*(\nu) = \mu'(\nu) + \mathrm{i}\mu''(\nu)$$

in the transition region, which are determined either by the Lorentzian,

$$\mu^*(\nu) = 1 + \sum_{k=1}^{3} \frac{\Delta\mu_k \nu_k^2}{\nu_k^2 - \nu^2 + \mathrm{i}\nu\Delta\nu_k}, \tag{1}$$

or the Gaussian,

$$\mu''(\nu) = \nu\left(\frac{\pi}{8}\right)^{1/2} \sum_{k=1}^{3} \Delta\mu_k \left\{ \exp\left[-\frac{(\nu-\nu_k)^2}{2\sigma_k^2}\right] + \exp\left[-\frac{(\nu+\nu_k)^2}{2\sigma_k^2}\right]\right\}, \tag{2a}$$

$$\mu'(\nu) = 1 + \frac{2}{\pi}\int_0^\infty \frac{\nu_1 \mu''(\nu_1)}{\nu_1^2 - \nu^2}\,\mathrm{d}\nu_1, \tag{2b}$$

lineshapes. Here, ν_k is the resonance frequency of the lines, $\Delta\nu_k$ (σ_k) is the Lorentzian (Gaussian) linewidth, and $\Delta\mu_k$ is the mode contribution to the static permeability, which determines the line intensities. Equation (2b) determines the real part of magnetic susceptibility in terms of the imaginary part through the Kramers–Krönig relation. The results derived from describing the transmission spectra in the vicinity of the $|\pm 10\rangle \rightarrow |\pm 9\rangle$ transition on the basis of the data of the alternative models (1) and (2) (Fig. 2a) clearly show that the

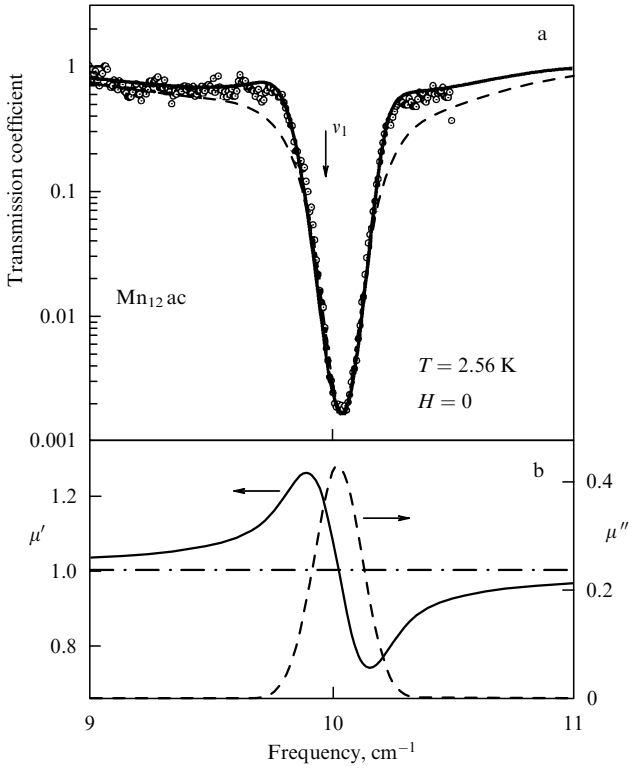

Figure 2. Transmission spectrum of a pellet pressed of a powder of Mn_{12}ac, near the $|\pm 10\rangle \rightarrow |\pm 9\rangle$ transitions at $H = 0$, illustrating (a) the description of the absorption line by the Gaussian (solid curve) and Lorentzian (dashed curve) lineshapes, and (b) the corresponding dispersion of the complex permeability for the Gaussian lineshape.

lineshape of the observed electronic transitions is Gaussian. This suggests that the linewidth is determined by the random (Gaussian) distributions of intracrystalline interactions, in particular, by internal magnetodipole and hyperfine fields, and also by a small spread of the crystal field related to random local stresses in the crystallites. For mode *1*, the Gaussian linewidth (dispersion) amounts to $\sigma_1 \approx 0.1$ cm (0.107 T), and the full width at half-maximum is $\Delta\nu_1 = 2(2\ln 2)^{1/2}\sigma_1 \approx 2.35\sigma_1 \approx 0.235$ cm^{-1} (0.252 T). The widths of the other transitions between the excited states amount to approximately the same value or are slightly smaller. The same Gaussian lineshapes of the transitions are observed for Fe_8 nanoclusters [24]. Recently, a group of researchers [30] carried out a detailed investigation of the various contributions to the inhomogeneous broadening of the transitions (the distribution of dipole fields, the *g* factor, and the crystal field). They studied Mn_{12}ac and Fe_8 by the EPR method and established, among other things, the important role of the distribution of the crystal field caused by local stresses. Note that mechanisms of electronic-transition-line broadening may also prove to play an important role in processes related to resonant tunneling of magnetization in nanoclusters.

The temperature dependences of the mode contributions, $\Delta\mu_k(T)$, calculated on the basis of the crystal field parameters, are in good agreement with the corresponding contributions found by directly simulating the transmission spectra, which is an independent proof that our results are correct, allowing for the absence of additional adjustable parameters (for more details, see Ref. [23]). Note that the absence of any additional lines above 10 cm^{-1} in the case of the sum frequencies $\nu_i + \nu_j$, which could correspond to forbidden transitions with $|\Delta m| > 1$, also supports the above structure of the quantum states of Mn_{12}ac. An interesting feature is the broad absorption band we observed in the high-frequency part of the absorption spectra ($\nu \geqslant 33$ cm^{-1}), which could be related to transitions to excited multiplets with $S \neq 10$. Such transitions have been detected in Mn_{12}ac by inelastic neutron scattering at frequencies of roughly 40 and 70 cm^{-1} [22]. In view of the fact that such transitions are spin-forbidden at $q = 0$, the question of the mechanism of their allowance arises, and this will require additional studies.

Let us now consider the spectroscopic properties of Mn_{12}ac in long-lived nonequilibrium states and the corresponding relaxation phenomena. In our experiments, we produced such states by cooling the sample to 3–1.8 K in a dc magnetic field that was perpendicular to the direction of propagation of radiation, and then rapidly ($\leqslant 1$ min) reversing the field direction. The magnitude of the field was not changed. Figure 3a shows examples of the time evolution of the transmission spectra at $T = 2.6$ K in a 0.45-T field. In the initial equilibrium state, the field, which splits the ground $|\pm 10\rangle$ and excited $|\pm 9\rangle$ doublets, produces an inhomogeneous line broadening for the polycrystalline sample and a shift in the transition frequency to the right of the initial line $\nu_0(H = 0) \approx 10$ cm^{-1} to $\nu_+ \sim 10.3$ cm^{-1}. Upon field reversal, the resonance frequency is shifted in the opposite direction from the initial line ν_0 to $\nu_- \sim 9.8$ cm^{-1}. This spectrum corresponds to the initial time $t = 0^+$, starting at which the spectra begin to relax and the intensity of the line ν_- decreases and that of the line ν_+ increases. With the passage of time, the line ν_- disappears and the initial line ν_+ is restored. Since the time during which the spectra are recorded (~ 30 s) is short compared to the overall relaxation time (~ 1000 s), we can ignore the changes in the spectra that occur during the recording process and assume the process to run instantly.

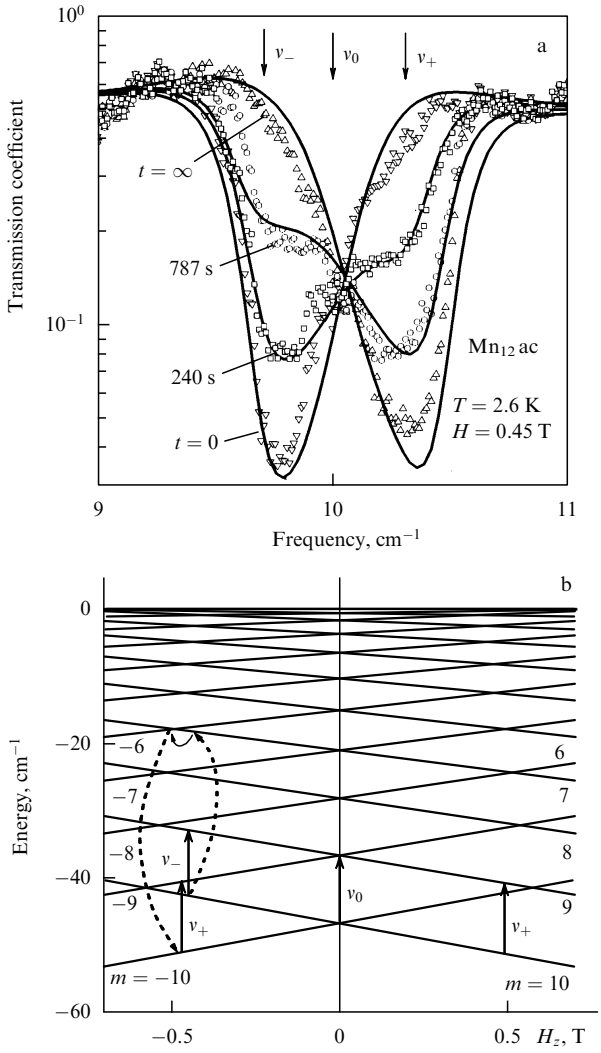

Figure 3. (a) Time evolution of the transmission spectra of a plane-parallel Mn_{12}ac pellet ($d = 1.39$ mm) caused by reversal of the magnetic field from +0.45 T to −0.45 T (the magnetic field is perpendicular to the direction in which the radiation propagates). The points represent the experimental data, and the lines represent the results of calculations with an effective relaxation time $\tau = 600$ s. The arrows mark the positions of the absorption lines in a zero field and in the fields $H = \pm 0.45$ T. (b) The energy levels of Mn_{12}ac placed in a magnetic field that is parallel to the easy axis, $H \| C_4$. The vertical arrows show the $|\pm 10\rangle \rightarrow |\pm 9\rangle$ transitions before and after field reversal. The curved arrows indicate possible relaxation paths for the transition of Mn_{12}ac from the metastable state to the ground state, a path that includes thermally activated transitions to the excited states and tunneling between coinciding levels.

The observed behavior of the spectra can be interpreted as follows. In the crystal and external magnetic fields, the quantum states of Mn_{12}ac are determined by the Hamiltonian

$$H_{\text{eff}} = D_2 S_z^2 + D_4 S_z^4 + B_4^4 \frac{S_+^4 + S_-^4}{2} - g\mu_B \mathbf{S} \cdot \mathbf{H}. \qquad (3)$$

The corresponding energy spectrum (Fig. 3b) in fields $H \ll H_A \approx 8$ T is mainly determined by the H_z component of the field, whose direction coincides with the easy axis C_4:

$E_m \approx D_2 m^2 + D_4 m^4 - g\mu_B m H_z$, where $m = 0, \pm 1, \ldots, \pm 10$. At low temperatures and $H_z > 0$ ($H_z < 0$) only one state is populated, namely, $|+10\rangle (|-10\rangle)$. Hence, there can be one transition $|+10\rangle \to |+9\rangle$ at the frequency $\nu_+ = \nu_0 + g\mu_B H_z > \nu_0$ ($H_z > 0$), which is observed in the transmission spectra in the equilibrium state (Fig. 3a). Field reversal ($H_z < 0$) transforms the spectrum, and the frequency of the $|+10\rangle \to |+9\rangle$ transition drops to $\nu_- = \nu_0 - g\mu_B |H_z| < \nu_0$. This is reflected in the shift of the line from ~ 10.3 to 9.8 cm^{-1} in Fig. 3a. Since the state $|+10\rangle$ becomes metastable after field reversal, its population relaxes to a new ground state $|-10\rangle$. As the population of this state increases, a new mode appears in the transmission spectra, corresponding to the transition $|-10\rangle \to |-9\rangle$ with the frequency $\nu_+ = \nu_0 + g\mu_B |H_z| > \nu_0$ ($H_z < 0$), while the intensity of the low-frequency mode ν_- decreases (Fig. 3a). With the passage of time, the initial spectrum with one line $\nu_+ > \nu_0$ is restored, with the line now corresponding to the transition $|-10\rangle \to |-9\rangle$ and the ground state with the opposite orientation of the magnetization. Strictly speaking, the above picture corresponds to the behavior of a single-crystal sample (or a single crystallite) in a field. For a polycrystalline sample, we should average the results over all orientations of the crystallites, which, however, does not change the qualitative picture of this phenomenon.

We now turn to the results obtained at lower temperatures (1.96 K) and in stronger fields (0.9 T), which demonstrate new features of the relaxation of the spectra (Fig. 4). Obviously, in this case the relaxation that follows the field reversal occurs 'nonuniformly' over the spectrum and is strongly frequency-dependent. Against the background of a general slowdown of relaxation (when there is practically no relaxation), there are two regions, one at $\nu_-^{(1)} = 9.57(2)$ cm^{-1} and the other at $\nu_+^{(1)} = 10.47(2)$ cm^{-1}, near which the transmission relaxation is relatively rapid: there is a peak in transmission at $\nu_-^{(1)}$ and a dip at $\nu_+^{(1)}$. We attribute this to resonant quantum tunneling in the crystallites of the polycrystalline Mn_{12}ac sample whose orientations with respect to the external field of a given magnitude correspond to the first level coincidence. As is known [3], this happens when $H_z^{(1)} \approx 0.45$ T, which corresponds to frequencies $\nu_\pm^{(1)} = \nu_0 \pm g\mu_B H_z^{(1)}$, in good agreement with positions of the dip and peak in the transmission coefficient. Moreover, taking into account that

$$H_z^{(1)} = -\frac{D_2 + D_4\left[m^2 + (m-1)^2\right]}{g\mu_B}$$

and that the corresponding frequencies $\nu_\pm^{(1)}$ depend on the number of coinciding levels of the quantum states $|m\rangle$ and $|-m+1\rangle$ ($m = 1, 2, \ldots, 9, 10$) because of a small contribution D_4 of fourth-order axial anisotropy, we can concretize the excited states of the cluster through which the main process of thermally activated tunneling at a given temperature and field runs. Note that the observed effects associated with the formation in the transmission spectra of a tunneling dip (peak) are in some sense similar to the spectral 'hole burning' in insulators (e.g., see Ref. [31]) and in our case they are caused by the formation of a 'hole' in the angular distribution of magnetization, with the position of the hole determined by the condition for level crossing in some of the crystallites of the polycrystalline sample.

Quantitative analysis of the observed relaxation phenomena requires calculating the effective permeability of the polycrystalline sample. In our calculations, we took into account (a) the nonequilibrium, time-dependent population of the quantum states of the clusters and (b) the inhomogeneous broadening of the $|\pm 10\rangle \to |\pm 9\rangle$ transitions in a magnetic field. We begin with the permeability $\mu(\nu, t)$ of a single crystallite in a nonequilibrium state, characterizing the state by the normalized populations $\rho_m(t)$ of states $|m\rangle$, i.e., by the diagonal elements of the corresponding density matrix that meet the condition

$$\Sigma \rho_m(t) = 1 .$$

Generalizing the equilibrium permeability used above, we can represent the transverse components of the permeability of interest to us with allowance for the states $m = \pm 10, \pm 9$ in the form

$$\begin{aligned}\mu_{xx}(t) = \mu_{yy}(t) = \mu_\perp(t) \\ = 1 + \Delta\mu^+(t)R^+(\nu) + \Delta\mu^-(t)R^-(\nu) \\ \equiv 1 + \Delta\mu_0\left[\frac{\nu_0}{\nu_+}(\rho_{10} - \rho_9)R^+(\nu) + \frac{\nu_0}{\nu_-}(\rho_{-10} - \rho_{-9})R^-(\nu)\right],\end{aligned} \tag{4}$$

where $\Delta\mu^\pm(t)$ is the time-dependent contribution of the transitions to the static permeability, which at $H = 0$ and

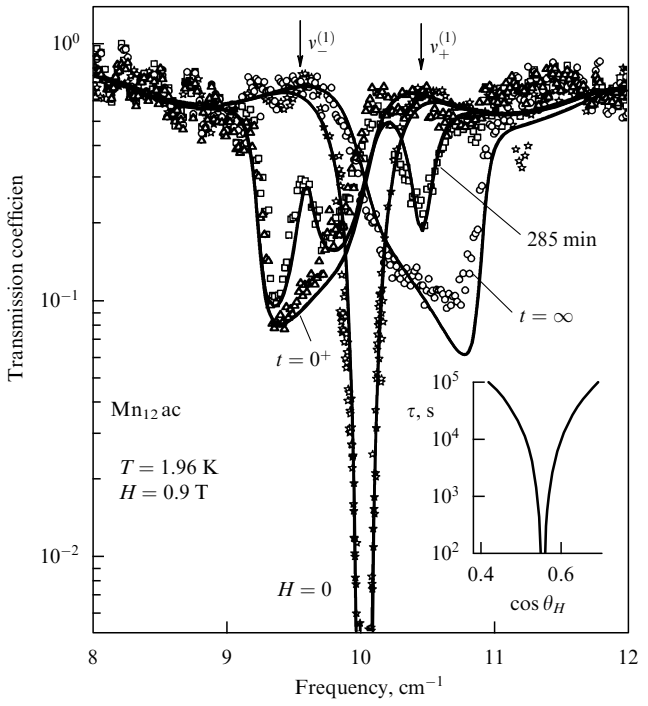

Figure 4. Time evolution of the transmission spectra of an Mn_{12}ac pellet at $T = 1.96$ K caused by reversal of the magnetic field from +0.9 T to −0.9 T. The peak at $\nu_-^{(1)}$ and the dip at $\nu_+^{(1)}$ in the transmission coefficient (indicated by arrows at the top of the figure) result from resonant tunneling for those Mn_{12}ac nanoclusters for which the energy levels of states with different directions of spin coincide. The points represent the experimental data, and the lines are the results of calculations with an effective relaxation time τ that resonantly depends on the orientation θ_H of the easy axis of a crystallite relative to the external field in the polycrystalline sample. The function $\tau(\theta_H)$ is shown in the inset; the central narrow line corresponds to $H = 0$.

$T = 0$ is

$$\Delta\mu_0 = 4\pi\chi_\perp^0 = 8\pi\rho N g^2 \mu_B^2 \frac{\left|\langle 10|S_{x,y}|9\rangle\right|^2}{\nu_0};$$

$$R_\pm(\nu) = \frac{\nu_\pm^2}{\nu_\pm^2 - \nu^2 + i\nu\Gamma_\pm}$$

is a function determining the lineshape, which for the sake of simplicity is assumed to be Lorentzian; $\nu_\pm = E_{\pm 9} - E_{\pm 10} = \nu_0 \pm g\mu_B H_z$ are the resonance frequencies of the $|\pm 10\rangle \to |\pm 9\rangle$ transitions in the field; N is the number of molecules per gram; and ρ is the density of the sample. In the equilibrium state, we have

$$\rho_m(t \to \infty) \equiv \rho_m^\infty = \frac{\exp(-\beta E_m)}{Z},$$

where $Z = \sum \exp(-\beta E_m)$, and $\beta = 1/k_B T$.

Generally, the time dependence of ρ_m is determined by the kinetic equations for all 21 states of the multiplet, which for Mn_{12}ac has been analyzed in Refs [32–34]. For the slowest part of the relaxation processes, which is of special interest to us, these equations can be reduced to one simple equation for the difference in the populations of the ground state, $\Delta\rho = \rho_{10} - \rho_{-10}$, with the effective relaxation time τ:

$$\frac{d\Delta\rho}{dt} = -\frac{\Delta\rho - \Delta\rho^\infty}{\tau}, \tag{5}$$

where

$$\Delta\rho^\infty \equiv \rho_{10}^\infty - \rho_{-10}^\infty = \frac{\exp(-\beta E_{10}) - \exp(-\beta E_{-10})}{Z}$$

is the equilibrium population difference for the reversed magnetic field ($\mathbf{H} \to -\mathbf{H}$). The solution of this equation for the initial condition $\Delta\rho(0) \equiv \Delta\rho^0 = -\Delta\rho^\infty$ corresponding to the nonequilibrium state that sets in after rapid field reversal yields

$$\Delta\rho(t) = \Delta\rho^\infty\left[1 - 2\exp\left(-\frac{t}{\tau}\right)\right]$$

and determines the population differences required by Eqn (4):

$$\Delta\rho_\pm(t) \equiv \rho_{\pm 10}(t) - \rho_{\pm 9}(t) = \Delta\rho_\pm^\infty + (\Delta\rho_\pm^0 - \Delta\rho_\pm^\infty)\exp\left(-\frac{t}{\tau}\right), \tag{6}$$

where

$$\Delta\rho_\pm^0 = \left\{1 \mp \Delta\rho^\infty[1 + \exp(-\beta\nu_\mp)]\right\} \times \frac{1 - \exp(-\beta\nu_\pm)}{2 + \exp(-\beta\nu_+) + \exp(-\beta\nu_-)},$$

$$\Delta\rho_\pm^\infty \equiv \rho_{\pm 10}^\infty - \rho_{\pm 9}^\infty = \frac{\exp(-\beta E_{\pm 10}) - \exp(-\beta E_{\pm 9})}{Z}.$$

All the quantities in Eqn (6) refer to the reversed field. In deriving these results, we assumed that the states $|\pm 10\rangle$ and $|\pm 9\rangle$ are in equilibrium: $\rho_{\pm 9} = \rho_{\pm 10}\exp(-\beta\nu_\pm)$. For low temperatures T, when $\rho_{\pm 9}$ is negligible, Eqn (6) becomes simpler:

$$\Delta\rho_\pm(t) \approx \rho_{\pm 10}(t) \approx \rho_\pm^\infty + (\rho_\mp^\infty - \rho_\pm^\infty)\exp\left(-\frac{t}{\tau}\right).$$

To apply these results to the polycrystalline sample, we must average the permeability (4) of individual crystallites over the different directions of their easy axes θ_H with respect to the field. The result is

$$\mu_\perp^{\text{eff}}(\nu, t) = \frac{1}{4}\int_0^\pi \mu_\perp(\nu, t, \theta_H)(1 + \cos^2\theta_H)\sin\theta_H\, d\theta_H. \tag{7}$$

This effective permeability is used to simulate the transmission spectra. First, we note that knowing $\mu_\perp^{\text{eff}}(\nu, t)$ makes it possible to describe the observed inhomogeneous broadening of the transitions, the changes in the line shape in a magnetic field in the initial and final stationary (equilibrium) states corresponding to $t = 0^-$ and $t = \infty$, and the transformation directly at the initial time ($t = 0^+$) after field reversal (Figs 3 and 4), with the use of the same values of frequency, linewidth, and contribution to static permeability as those obtained for a zero field ($\nu_0 = 10.02$ cm^{-1}, $\Gamma = 0.182$ cm^{-1}, and $\Delta\mu_0 = 0.01065$ at $T = 2.6$ K). To allow for the small asymmetry of the spectra with respect to ν_0, observed when the field is reversed, we took into account the small contribution to the external field that arises from the internal dipole fields, $\lambda M \approx 0.04 - 0.05$ T, where M is the magnetization of Mn_{12}ac.

We now examine the time evolution of the spectra in nonstationary states, which are mainly determined by the relaxation time $\tau = \tau(\theta_H, H, T)$. At $T = 2.6$ K in a moderate external field, spectrum relaxation is basically described by a relaxation time τ that does not depend on θ_H (Fig. 3a), in which case the populations ρ_m depend exponentially on the time. However, as the field strength grows, the function $\rho_m(t)$ deviates considerably from the exponential function, which arises from the distribution of relaxation times in a polycrystalline sample, i.e., their dependence on θ_H. These effects manifest themselves even more strongly at $T = 1.96$ K in a 0.9 T field, where we are actually dealing with a resonance dependence of relaxation time on θ_H due to resonance tunneling. Let us study this problem more thoroughly, based on the recent theoretical investigations of thermally activated relaxation processes in Mn_{12}ac [32–34], which allow for spin–phonon interaction and resonance tunneling involving excited states. Generally, relaxation in such a multilevel system is determined by the various relaxation paths involving all the excited states, and its analysis requires the use of numerical methods. If we limit ourselves to the resonance behavior of $\tau(\theta_H, H, T)$ near the first crossing of levels m and $m' = -m + 1$, we can use the simple model of Leuenberger and Loss [33] and Pohjola and Schoeller [34], within which the relaxation time is given by the sum

$$\tau \approx \tau_{S,m} + \tau_{mm'} + \tau_{m',-S},$$

where

$$\tau_{S,m} \approx \tau_{m',-S} \approx \frac{\exp(\beta E_{m+1})}{Z_S}\frac{1}{W_{mn}},\ n = m \pm 1,\quad m = \pm 2$$

are the relaxation times for the transitions $S \to m$ and $m' \to -S$, respectively, W_{mn} is the probability of the $n \to m$ transition determined by the spin–phonon interaction, and

$$Z_S = \exp(\beta E_S) + \exp(\beta E_{-S}).$$

Here,

$$\tau_{mm'} = \frac{\exp(\beta E_m)}{Z_S}\,\frac{1}{\Gamma_{mm'}}$$

is the relaxation time of the tunneling transition $m \to m'$, where

$$\Gamma_{mm'} = \frac{E_{mm'}^2 (W_m + W_{m'})}{4(E_m - E_{m'})^2 + \hbar^2 (W_m + W_{m'})^2}$$

is the rate of transition between m and m', with $E_{mm'}$ the tunneling splitting of levels m and m', and

$$W_m = \sum_n W_{nm}$$

is the width of level E_m determined by the spin–phonon interaction (the levels E_m have been defined earlier). Assuming that $W_m + W_{m'} \approx 2W_{mm+1} \equiv 2W_{\rm ph}$ and that the quantities $W_{\rm ph}$ and $E_{mm'} \equiv E_{\rm T}$ are variable parameters, we simulated the transmission spectra with allowance for the resonance behavior of $\tau(\theta_H)$ (the inset in Fig. 4), which made it possible to describe their observed time evolution at $T = 1.96$ K (see Fig. 4) and to estimate $E_{\rm T}$ and $W_{\rm ph}$, which were found to be approximately $0.0025\ {\rm cm}^{-1}$ and $5 \times 10^8\ {\rm s}^{-1}$, respectively. Here, the observed positions of the dip and peak, $v_{\pm}^{(1)}$, localize the excited states through which the tunneling takes place at $m = 7$ and $m' = -6$ (or $m = 6$ and $m' = -7$) or at least at values close to these if we allow for errors in determining $v_{\pm}^{(1)}$. Strictly speaking, one should simultaneously take into account several relaxation paths, which produce, respectively, several adjacent resonances in $\tau(\theta_H)$. This has been corroborated by our calculations of $\tau(\theta_H)$ based on the numerical solution of the kinetic equations of all 21 states of the ground Mn_{12}ac multiplet, which also show that, as m increases, the resonance dips in $\tau(\theta_H)$ become much narrower and shallower. The dips have a Lorentzian shape and an effective width $\Gamma_{\rm eff} \sim \max[E_{mm'}, \hbar(W_m + W_{m'})]$, i.e., one determined either by tunneling splitting or by the width of transitions caused by the spin–lattice interaction. However, under conditions of inhomogeneous level broadening characterized by dispersion σ, the shape of the resonances may become Gaussian under appropriate averaging and when $\sigma \gg \Gamma_{\rm eff}$. Indeed, the linewidth of the $m \to n$ transitions, which is related to the spin–lattice interaction $\Gamma_{mn}^{\rm ph} = \hbar(W_m + W_n)$ and determines the tunneling rate $\Gamma_{mm'}$, amounts to $\sim 10^{-4} - 10^{-2}\ {\rm cm}^{-1}$, which is much smaller than the real width related to inhomogeneous broadening. Hence, when $E_{mm'} > \hbar(W_m + W_{m'})$, the width and shape of the resonances in $\tau(\theta_H)$ are Lorentzian for $E_{mm'} > \sigma$ and Gaussian for the opposite case. However, in a polycrystalline sample, this fine resonance structure in $\tau(\theta_H)$ apparently becomes strongly smeared, and its manifestation in the relaxation of transmission spectra may be strongly suppressed. These problems will be treated in a separate publication.

In conclusion, using a single method — submillimeter BWO spectroscopy — we have studied (a) the structure of the lower energy levels of the Mn_{12}ac nanocluster and its interaction with the surroundings (the frequency, width, and shape of the lines of electronic transitions), and (b) the relaxation of long-lived spin states within the ground multiplet of the cluster. At low temperatures ($T < 2$ K), a spectrally inhomogeneous relaxation is observed, which manifests itself in the formation of a *tunneling dip* in one part of the transmission spectrum and of a corresponding peak in another. We have found that the effect is caused by resonance tunneling of the magnetization of that fraction of the Mn_{12}ac clusters in which the energy levels of states with opposite directions of spin coincide. We have proposed a theoretical model that makes it possible to describe these phenomena by allowing for the time evolution of the populations of spin states, the inhomogeneous broadening of the electronic transitions, and the resonance nature of relaxation due to magnetization tunneling.

This work was supported by the Russian Foundation for Basic Research (Project No. 02-02-16597), the Quantum Macrophysics Program of the Russian Academy of Sciences, and Deutsche Forschungsgemeinschaft.

References

1. Sessoli R et al. *Nature* **365** 141 (1993)
2. Gatteschi D et al. *Science* **265** 1054 (1994)
3. Thomas L et al. *Nature* **383** 145 (1996)
4. Friedman J R et al. *Phys. Rev. Lett.* **76** 3830 (1996)
5. Hernandez J M et al. *Europhys. Lett.* **35** 301 (1996)
6. Hartmann-Boutron F, Politi P, Villain J *Int. J. Mod. Phys. B* **10** 2577 (1996)
7. Barbara B, Gunther L *Phys. World* **12** (3) 35 (1999)
8. Caneschi A et al. *J. Magn. Magn. Mater.* **200** 182 (1999)
9. Barbara B et al. *J. Magn. Magn. Mater.* **200** 167 (1999)
10. Wernsdorfer W, Sessoli R *Science* **284** 133 (1999)
11. Sangregorio C et al. *Phys. Rev. Lett.* **78** 4645 (1997)
12. Lionti F et al. *J. Appl. Phys.* **81** 4608 (1997)
13. Zvezdin A K *Priroda* (12) 11 (2000); Zvezdin A K, Zvezdin K A *Priroda* (9) 9 (2001)
14. Leuenberger M N, Loss D *Nature* **410** 789 (2001)
15. Tejada J et al. *Nanotechnology* **12** 181 (2001)
16. Paulsen C et al. *J. Magn. Magn. Mater.* **140 – 144** 379 (1995)
17. Chiorescu I et al. *Phys. Rev. Lett.* **85** 4807 (2000)
18. Bokacheva L, Kent A D, Walters M A *Phys. Rev. Lett.* **85** 4803 (2000)
19. Zhong Y et al. *Phys. Rev. B* **62** R9256 (2000)
20. Barra A L, Gatteschi D, Sessoli R *Phys. Rev. B* **56** 8192 (1997)
21. Hill S et al. *Phys. Rev. Lett.* **80** 2453 (1998)
22. Hennion M et al. *Phys. Rev. B* **56** 8819 (1997); Mirebeau I et al. *Phys. Rev. Lett.* **83** 628 (1999)
23. Mukhin A A et al. *Europhys. Lett.* **44** 778 (1998); *Physica B* **284 – 288** 1221 (2000)
24. Mukhin A et al. *Phys. Rev. B* **63** 214411 (2001)
25. *Submillimetrovaya Dielektricheskaya Spektroskopiya Tverdogo Tela* (Submillimeter Dielectric Spectroscopy of Solids) (Proc. (Trudy) of General Physics Institute of Russ. Acad. Sci., Vol. 25, Ed. G V Kozlov) (Moscow: Nauka, 1990)
26. Kozlov G V, Volkov A A, in *Millimeter and Submillimeter Wave Spectroscopy of Solids* (Topics in Appl. Phys., Vol. 74, Ed. G Grüner) (Berlin: Springer, 1998) p. 51
27. Dressel M et al., cond-mat/0110340 (v1)
28. Sessoli R et al. *J. Am. Chem. Soc.* **115** 1804 (1993)
29. Born M, Wolf E *Principles of Optics* 7th ed. (Cambridge: Cambridge Univ. Press, 1999)
30. Park K et al. *Phys. Rev. B* **65** 014426 (2002); Hill S et al. *Phys. Rev. B* **65** 224410 (2002)
31. *Proc. of the 6th Intern. Conf. on Hole Burning and Related Spectroscopies* (Ed. J-P Galaup); *J. Lumin.* **86** (2000)
32. Garanin D A, Chudnovsky E M *Phys. Rev. B* **56** 11102 (1997)
33. Leuenberger M N, Loss D *Phys. Rev. B* **61** 1286 (2000)
34. Pohjola T, Schoeller H *Phys. Rev. B* **62** 15026 (2000)